Heat Capacity and Anisotropic Thermal Conductivity in Cr 2 AlC Single Crystals at High Temperature

A. Champagne, J.-L. Battaglia, T. Ouisse, F. Ricci, A. Kusiak, Christophe Pradere, V. Natu, A. Dewandre, M. Verstraete, M. Barsoum, et al.

Heat Capacity and Anisotropic Thermal Conductivity in Cr 2 AlC Single Crystals at High Temperature

Article *in* The Journal of Physical Chemistry C · October 2020

DOI: 10.1021/acs.jpcc.0c08384

11 authors, including:

Aurélie Champagne
Université Catholique de Louvain - UCLouvain
11 PUBLICATIONS **65** CITATIONS
SEE PROFILE

Jean-Luc Battaglia
University of Bordeaux
197 PUBLICATIONS **1,800** CITATIONS
SEE PROFILE

Thierry Ouisse
Université Grenoble Alpes
178 PUBLICATIONS **2,404** CITATIONS
SEE PROFILE

Francesco Ricci
Université Catholique de Louvain - UCLouvain
35 PUBLICATIONS **385** CITATIONS
SEE PROFILE

Heat capacity and anisotropic thermal conductivity in Cr_2AlC single crystals at high temperature

A. Champagne,[1,*] J.-L. Battaglia,[2] T. Ouisse,[3] F. Ricci,[1] A. Kusiak,[2] C. Pradere,[2] V. Natu,[4] A. Dewandre,[5] M. J. Verstraete,[5] M. W. Barsoum,[4] and J.-C. Charlier[1]

[1]*Institute of Condensed Matter and Nanosciences, Université catholique de Louvain, B-1348 Louvain-la-Neuve, Belgium*

[2]*I2M Laboratory, UMR CNRS 5295, University of Bordeaux, 33405 Talence CEDEX, France*

[3]*Univ. Grenoble Alpes, CNRS, Grenoble INP, LMGP, F-38000 Grenoble, France*

[4]*Department of Materials Science and Engineering, Drexel University, Philadelphia, Pennsylvania-19104, United States*

[5]*CESAM-QMAT-nanomat, and European Theoretical Spectroscopy Facility, Université de Liège, B-4000 Sart-Tilman, Belgium*

(Dated: October 1, 2020)

Abstract

The temperature dependences of both heat capacity and thermal conductivity in nano-lamellar Cr_2AlC single crystals are measured using modulated photothermal radiometry and compared to first-principles calculations. The electronic contribution to the thermal conductivity of Cr_2AlC single crystals is computed *ab initio* by determining the electronic transport coefficients using density functional theory and by solving the Bloch-Boltzmann transport equation with a temperature-dependent relaxation time. The lattice thermal conductivity is predicted going beyond the quasi-harmonic approximation and considering renormalized second and third order force constant matrices, with anharmonic three-phonon scattering, isotopic scattering, and scattering by carbon vacancies. Isotopic scattering does not modify the lattice thermal conductivity. In contrast, even a small concentration of carbon vacancies induces a substantial decrease of the in-plane lattice thermal conductivity. The anisotropy measured in the thermal conductivity, with a ratio of ~ 2 over the whole temperature range, is confirmed theoretically. This anisotropy seems to mainly arise from lattice contributions. A similar anisotropy is expected for other MAX phases with identical layered structures.

Keywords: MAX single crystals, Thermal conductivity, Heat capacity, First-principles calculations, Modulated Photothermal Radiometry

I. INTRODUCTION

The MAX phases are layered, hexagonal, early transition metal carbides and nitrides, with formula $M_{n+1}AX_n$, where M represents an early transition metal, A an element from groups 13 to 16, X either carbon or nitrogen, and n varies from 1 to 3. There are currently more than 150 MAX phases known,[1,2] including both quaternary in- and out-of-plane ordered phases,[3–5] as well as the recently discovered rare-earth containing MAX phases.[6–8] In contrast to graphite-like layered materials, the MAX phases combine strong intralayer covalent/metallic MX bonds and weaker interlayer metallic MA bonds. In most cases, the atomic masses are very different - C atoms are light in comparison with the M and the A atoms - leading to a wide range of optical phonon energies.[9] By now, it is well established that at least a subset of MAX phases combine some of the best properties of metals and ceramics,[1,9,10] including high electrical and thermal conductivities, chemical, oxidation, and thermal shock resistances, as well as reversible deformation,[11] and bulk ripplocations.[12–16] The growing interest of the scientific community results both from their own intrinsic physical properties and from the possibility to exfoliate them to form a new family of two-dimensional materials, called MXenes.[17] Taken together, these characteristics give MAX phases their anisotropic properties. Pure MAX phases were synthesized for the first time in 1996,[18] but the lack of large single crystals has long prohibited a direct assessment of the anisotropy of the physical properties expected from their crystal structure [see Fig. 1(a)]. As a consequence, most of the studies on the electrical and thermal transport in MAX phases were performed on polycrystals.[19,20] Since 2011, macroscopic single crystals have been available,[21–24] and their magneto-transport properties have been investigated,[25,26] as well as their electronic structure[27] and elastic properties.[16]

Recently, the phonon dispersion branches of Cr_2AlC MAX phase single crystals have been obtained experimentally with neutron inelastic scattering and computed *ab initio* within the density functional perturbation theory (DFPT).[28] The anisotropy of the phonon branches has been predicted with a very satisfactory accuracy when compared to experiment, thus allowing for further investigation of the anisotropy of the thermal conductivity in these MAX single crystals.

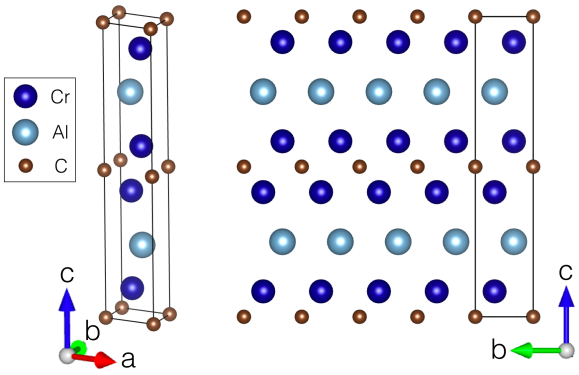

FIG. 1. Atomic structure of Cr_2AlC ($P6_3/mmc$ space group, $a = b = 0.286\,\text{nm}$, $c = 1.282\,\text{nm}$).

In this work, the heat capacity and the anisotropic thermal conductivity of Cr_2AlC single crystals are measured from room temperature (RT) up to 600°C. The experimental techniques are described in sections II A and II B, and the results are discussed in section III A. The measurements are compared to *ab initio* calculations and to fundamental analytic models including the Wiedemann-Franz law and the Callaway and Klemens models. The electronic and lattice contributions to the thermal conductivity are computed using the BoltzTraP2 code[29,30] and the temperature dependent effective potential (TDEP) code,[31–33] respectively. Computational details can be found in section II C. The theoretical predictions are presented in section III B, and all results are discussed in section IV. Finally, conclusions are drawn in section V.

II. METHODS

A. Crystal growth

Single crystalline platelets of Cr_2AlC are grown from a liquid solution of composition $x_{Cr} = 0.36$, $x_{Al} = 0.57$ and $x_C = 0.07$. After a temperature plateau at $T_{max} = 1650$°C for two hours to ensure carbon dissolution, the crystal growth is achieved by slowly cooling the solution from T_{max} down to $T = 1200$°C during time periods ranging from 5 to 7 days with an Ar pressure $p_{Ar} = 1.5\,\text{bar}$. Slow cooling aims at limiting unwanted spontaneous nucleation by putting to good use Ostwald ripening. The growth rate is much slower along the c-axis, resulting in a morphology with a low aspect ratio. The largest platelet areas are

around 6-10 cm^2 with thicknesses limited to 2 mm. Single crystals are cleaved and do not include grain boundaries. The crystal quality is checked by x-ray Laue transmission and through neutron diffraction. More details on the sample preparation and on their structure can be found in Ref.[28]

B. Electrical and thermal conductivity measurements

The Cr_2AlC single crystals are first cut with a diamond wire saw in order to obtain square-shaped samples of about $1 - 2\,cm^2$. They are then polished in order to obtain a uniform thickness of about 100 μm.

Four equidistant and parallel Cr/Au contact pads are deposited on the single crystals, as illustrated in Fig. 2. The initial Cr layer is 10 nm thick followed by $\sim$ 150 nm thick gold layer. Later, silica sheathed copper wires are attached to the gold pads using graphite glue (Ted Pella, USA). The whole assembly is placed inside a furnace under flowing Ar and the furnace is heated up to 700°C at 5°C per minute. The copper wire contacts coming out of the furnace are passed through a rubber stopper to protect the inert atmosphere inside. A 100 mA current is passed through the outer wires using a constant current source (Hewlett-Packard, DC current source, USA) and the voltage at the inner probes is recorded using a voltmeter (Keithley Instruments, USA). The correction factor used to correct the raw resistance data is a function of the sample geometry and is calculated according to Ref.[34].

The temperature dependence of the heat capacity was obtained using the differential scanning calorimetry (DSC) technique in the [RT-600]°C temperature range, with a heating rate of 10°C/minute.

Both in-plane and out-of-plane thermal conductivities of the Cr_2AlC samples are measured using the modulated photothermal radiometry (MPTR) within two distinct frequency ranges.[35] The characterization is performed in the [RT-600]°C temperature range under Ar flow. The MPTR method consists in submitting sample's surface to a periodic heat flux generated by a modulated laser. The increase in temperature leads to a modulated infrared (IR) radiation that is monitored using a HgCdTe IR detector. The amplitude and the phase are given using a lock-in amplifier. In addition, the in-plane thermal diffusivity at RT is measured using the pulsed flying spot (PFS) with the logarithmic parabolas method.[36] The out-of-plane thermal diffusivity at RT is also measured using the periodic pulse radiometry

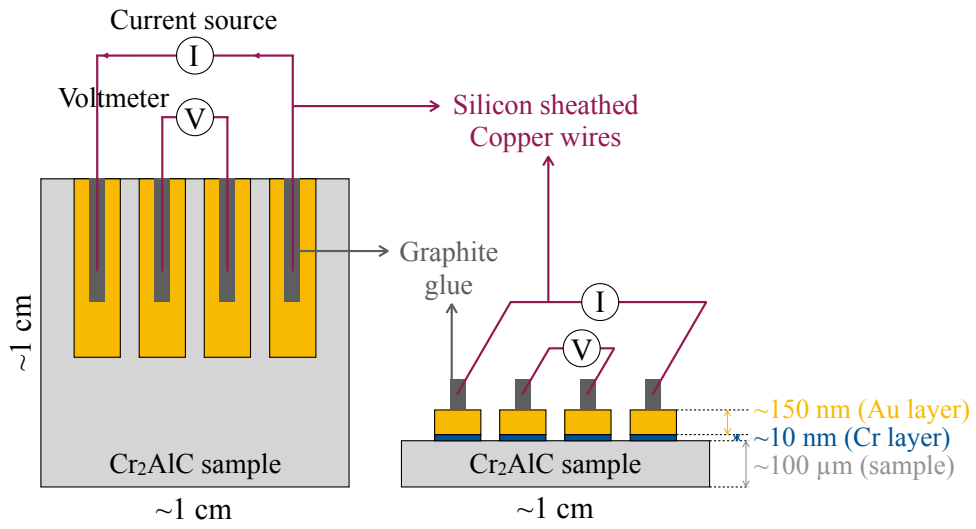

FIG. 2. Schematic of the in-plane resistivity measurements in Cr_2AlC using a four-probe configuration with equidistant and parallel pads.

technique (PPRT),[37] which consists of heating the front face of the sample using a periodic laser pulse and measuring the transient average temperature on the rear face using an IR detector. Similar to the MPTR method, the thermal diffusivity is identified by minimizing the quadratic gap between the experimental relative change in temperature and the one calculated from a model of the heat transfer within the PPRT experimental configuration. The minimization is performed using the Levenberg-Marquardt algorithm.

C. First-principles computational modeling

The structural, electronic, and vibrational properties are computed *ab initio* using density functional theory (DFT)[38,39] and density functional perturbation theory (DFPT),[40–44] respectively, using the ABINIT package[45–47] which is based on plane-wave basis sets to represent the Kohn-Sham orbitals and charge density. The exchange-correlation functional is approximated using the generalized gradient approximation as proposed by Perdew, Burke and Ernzerhof.[48] Optimized norm-conserving Vanderbilt pseudopotentials[49] are used to describe core-valence interaction. A plane-wave kinetic energy cut-off of 40 Hartree is determined through a careful convergence investigation. The first Brillouin zone is sampled with a $18 \times 18 \times 6$ Monkhorst-Pack k-point grid, and a Gaussian smearing of 1 mHa is used to accelerate the convergence. Both Fermi surface and Fermi velocities are obtained on a dense

homogeneous $72 \times 72 \times 72$ k-point grid and are visualzed using the Fermisurfer code.[50] The optimization of the cell parameters leads to an underestimation of the experimental values and thus to an overestimation of the high-frequency phonon modes, which is problematic in the study of transport properties. Following our previous work,[28] the lattice parameters are thus kept fixed at the experimental values for Cr_2AlC $a = 0.286\,\text{nm}$ and $c = 1.282\,\text{nm}$, and the atomic positions inside the unit cell are fully optimized until the largest force is smaller than $2.5 \times 10^{-4}\,\text{eV/Å}$.

The thermal conductivity can be decomposed into its electronic and lattice contributions, such that $\kappa = \kappa_e + \kappa_l$. The transport theory for electrons is implemented in the BoltzTraP2 code[29,30] which computes the electronic transport coefficients assuming rigid bands (unchanged either with doping or temperature) and usually a constant relaxation time τ_0. The estimation of the lattice contribution includes anharmonic processes and, hence, the computation of the third-order force constant matrix. The effective second- and third-order interatomic force constants (IFCs) are obtained at a given temperature from a fit of DFT forces in supercells with thermally displaced atoms (based on initial DFPT harmonic estimates) using the TDEP code.[31–33] The lattice thermal conductivity tensor and cumulative thermal conductivity are then obtained from the iterative solution of the phonon Bolzmann transport equation (BTE). External scattering processes are also considered, *i.e.*, vacancy, isotope, and grain boundary scattering processes. The isotopic concentrations are chosen to be as close as possible to the natural ones: carbon of 98.93% ^{12}C, 1.07% ^{13}C, aluminum of 100% ^{27}Al, and chromium of 4.35% ^{50}Cr, 83.79% ^{52}Cr, 9.50% ^{53}Cr, 2.36% ^{54}Cr. The determination of the phonon scattering rates due to three-phonon collisions and to extrinsic scattering processes using an *ab initio* approach is described in detail in Refs.[31–33].

III. RESULTS

A. Measurements

1. *Electrical resistivity*

In order to gain insight into the transport properties of Cr_2AlC single crystals, the in-plane electrical resistivity $\rho_{\parallel}(T)$ is measured experimentally, in the $[50-750]$°C temperature range, using a four-probe configuration as the one depicted in Fig. 2. The result is depicted

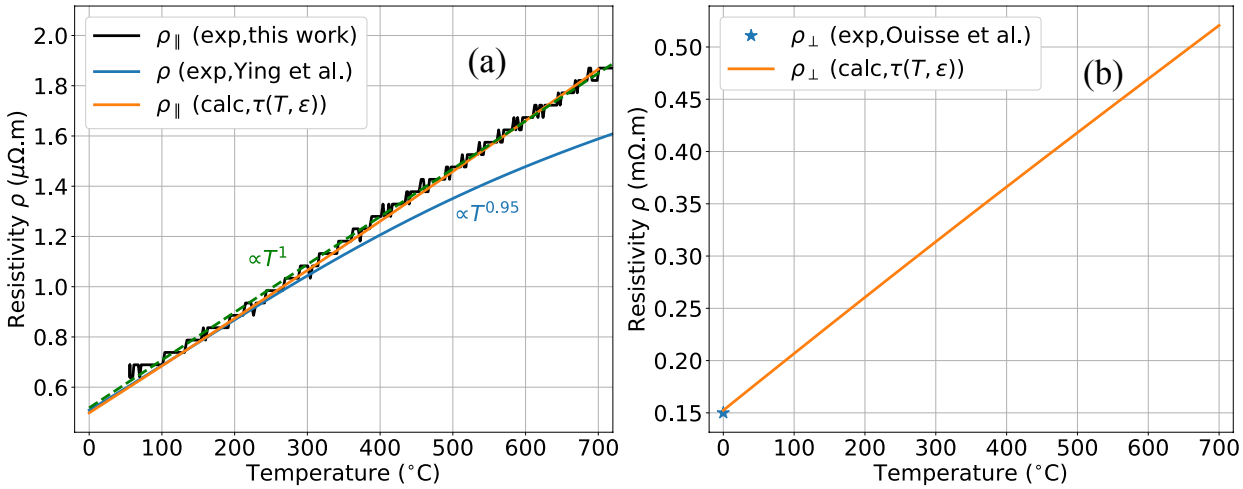

FIG. 3. (a) Temperature-dependence measurements of the in-plane resistivity $\rho_\parallel$ for Cr_2AlC single crystals (black line), compared to experimental data from Ref.[52] for a polycrystalline sample (blue line), and to the computed in-plane resistivity (orange line) using the relaxation time $\tau(T,\varepsilon)$ as defined in Eq. 15. The dashed green line is a guide to the eye, highlighting the linear temperature dependence of the resistivity. (b) Predicted out-of-plane resistivity (orange line) using $\tau(T,\varepsilon)$, compared to experimental data from Ref.[25].

in Fig. 3(a). Not surprisingly, a linear temperature-dependence is observed, as is usual in metals, due to the linear increase of the phonon occupation with temperature. This experimental curve will be further used to investigate the thermal transport in Cr_2AlC single crystals in Section III B 2. A value of $\sim 0.7\,\mu\Omega$m is obtained at 50°C, which is about ten times higher than the one previously measured by Ouisse *et al.*[25] This might be due to the configuration used to measured the resistivity where the contacts are all deposited on the top surface. On the other hand, it appears that the curve is close to previous reports for Cr_2AlC polycrystals with electrical resistivities ranging from 0.6 to $0.74\,\mu\Omega$m at 300 K.[51–53] It can be noted here that the electrical resistivity of Cr_2AlC is almost twice higher than the one of other M_2AlC systems.[9] For example, the electrical resistivities of Ti_2AlC,[54] V_2AlC,[51] and Nb_2AlC[51] are 0.36, 0.25, $0.29\,\mu\Omega$m, respectively, at 300 K.

2. *Heat capacity and thermal conductivity*

Both in-plane and out-of-plane thermal conductivities are measured using the MPTR technique with two distinct frequency ranges. At high (low) frequency, the measured phase is sensitive to the in-plane (out-of-plane) thermal diffusivity $a_{\parallel}$ ($a_{\perp}$). Using the measured density $\rho = 5210\,\mathrm{kg/m^3}$ and the temperature-dependent heat capacity $C_p(T)$ [see Fig. 4(a)], the temperature-dependent in-plane thermal conductivity $\kappa_{\parallel}(T)$ and out-of-plane thermal conductivity $\kappa_{\perp}(T)$ are obtained. $\kappa_{\parallel}(T)$ measured on several Cr_2AlC samples using the MPTR are depicted in gray in Fig. 4(b). A total of seven curves are reported among which four are increasing with T at high temperature and three are decreasing with T at high temperature. The deviations between the different gray curves may result from the variable quality of the different samples and the sensitivity of the measurements. They still provide results in the same order of magnitude, with an average thermal conductivity curve depicted in blue in the same figure. The out-of-plane thermal conductivity $\kappa_{\perp}(T)$ of a unique sample is measured and depicted in orange in Fig. 4(b). Values of $\kappa_{\parallel} = 41.3\,\mathrm{Wm^{-1}K^{-1}}$ and $\kappa_{\perp} = 21.6\,\mathrm{Wm^{-1}K^{-1}}$ are obtained at RT.

In addition, the in-plane thermal diffusivity at RT is measured using the PFS with the logarithmic parabolas method.[36] A value of $a_{\parallel} = 11.4\,\mathrm{mm^2/s}$ is measured, leading to a $\kappa_{\parallel} = 40.8\,\mathrm{Wm^{-1}K^{-1}}$ at RT. This PFS measurement is useful to validate the MPTR values. The temperature dependence of $\kappa_{\perp}$ is also measured using the PPRT technique and the results are reported in Fig. 4(b). These values confirm rather well those obtained with the MPTR technique, although the slight increase at the highest temperatures is not observed anymore. Given the high standard deviation on $\kappa_{\perp}$ using the MPTR technique, we suspect the increase is spurious. Comparisons with values of $\kappa_{\perp}$ in the literature are also reported in Fig. 4(b). The measurements obtained by Tian *et al.*[53] in a more narrow temperature range fit rather well with the present measurements. As a global observation, the in-plane thermal conductivity is found to be almost constant in the whole temperature range, whereas the out-of-plane thermal conductivity slightly decreases with increasing temperature and before saturating above 200°C. As importantly, an anisotropy ratio of about 2 is found over the whole temperature range.

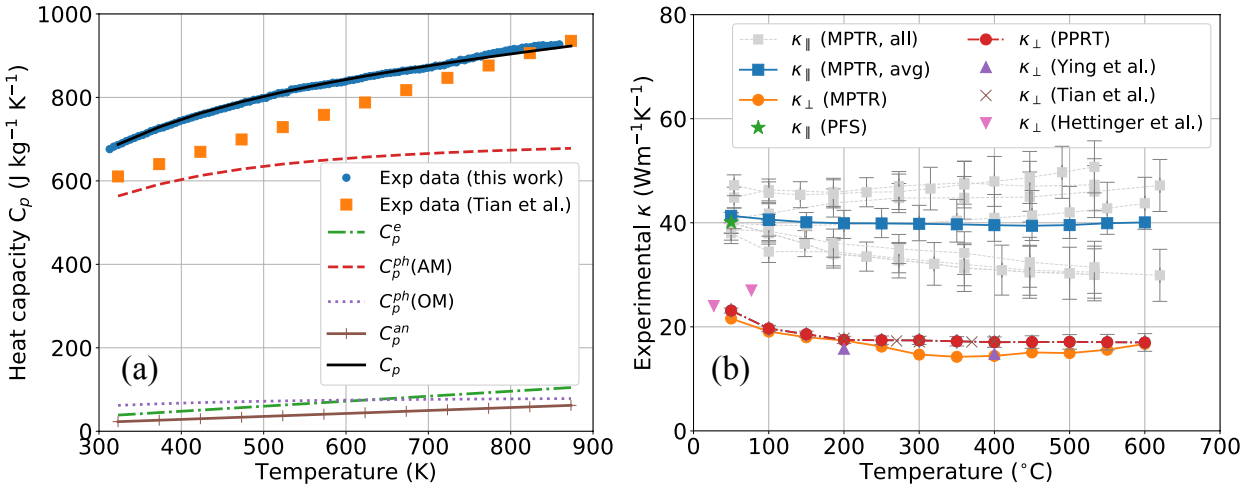

FIG. 4. (a) Heat capacity measurements of Cr_2AlC single crystal measured experimentally (blue dots), compared to experimental data from Ref.[55] (orange squares) and theoretical values (black solid line) obtained from electrons (C_p^e), acoustic and optical phonons [C_p^{ph}(AM), C_p^{ph}(OM)], and anharmonic (C_p^{an}) contributions. (b) Measured in-plane ($\kappa_\parallel$) and out-of-plane ($\kappa_\perp$) thermal conductivities using various techniques, compared to values found in the literature.[51–53] Error bars for MPTR and PPRT measurements are represented by dark gray lines.

B. Theoretical simulations

1. *Heat capacity*

The total heat capacity C_p is composed of several contributions, including the electronic part (from the metallic character of Cr_2AlC), the lattice part, and the anharmonic scattering that occurs at high temperature:[61]

$$C_p = C_p^e + C_p^{ph} + C_p^{an} \tag{1}$$

where

$$C_p^e = \frac{\pi^2 k_B^2 N(E_F)}{3 q_e N_A} T \tag{2}$$

is the electronic contribution with $N(E_F)$ denoting the density of states (DOS) at the Fermi energy E_F. The phonon contribution $C_p^{ph} = C_p^{ph}(\mathrm{AM}) + C_p^{ph}(\mathrm{OM})$ is accounted with both the acoustic modes (AM) and the optical modes (OM). Assuming all the atoms are involved equally within the AM, the contribution of AM is conventionally expressed from the phonon

TABLE I. Theoretical and experimental values used to model the heat capacity and the thermal conductivity of the Cr_2AlC MAX phase.

Cr_2AlC	Parameter description(s)	Value(s)	Refs.
M [g mol^{-1}]	Molar mass	52(Cr)/27(Al)/12(C)	
a [Å] - c [Å]	Lattice constants	2.863 - 12.814	Exp.[56–58]
V_0 [Å^3]	Volume of the elementary cell	90.6	Exp.[56,57]
ρ [kg m^{-3}]	Density	5210	Exp.
L [cm]	Grain size (@300 K)	$\sim 1-2$	This work
α_V [K^{-1}]	Thermal expansion coefficient	11.2×10^{-6}	Exp.[58,59]
B [GPa]	Bulk modulus	226	Calc.[56,57,59,60]
Θ_E [K]	Einstein temperature	260, 320, 925	Exp.[19]
Θ_D [K]	Debye temperature	675	This work
γ [J mol^{-1} K^{-2}]	Temperature coeff. of C_p^e	17.15×10^{-3}	Exp.[19]
G	Grüneisen parameter ($= 3B\alpha_V/C_p$)	1.5	Calc.[58]
v_{T_1}/v_{T_2} [m s^{-1}]	Transverse sound velocities along		
	$\Gamma-M$	4820/5216	Calc.[28]
	$\Gamma-K$	4820/5216	Calc.[28]
	$\Gamma-A$	5056/5056	Calc.[28]
v_L [m s^{-1}]	Longitudinal sound velocity along		
	$\Gamma-M$	7664	Calc.[28]
	$\Gamma-K$	7664	Calc.[28]
	$\Gamma-A$	9566	Calc.[28]
$N(E_F)$ [(eV.unit cell)$^{-1}$]	Density of states at the Fermi level	6.46	Exp.[60]
E_F [eV]	Fermi energy	8.07	Calc.[57]

DOS $D_p(\omega)$ given, within the Debye approximation, by

$$D_p(\omega) = \frac{\omega^2}{2\pi^2 v^3} \tag{3}$$

with

$$v = 3^{1/3}\left(\frac{1}{v_L^3} + \frac{2}{v_T^3}\right)^{-1/3} \tag{4}$$

the sound velocity, as:

$$C_p^{ph}(\mathrm{AM}) = \frac{\hbar^2}{k_B T^2} \int_0^{\omega_D} \frac{\omega^2 e^{\frac{\hbar\omega}{k_B T}}}{\left(e^{\frac{\hbar\omega}{k_B T}} - 1\right)^2} D_p(\omega) d\omega \tag{5}$$

$$= 9 N k_B \frac{T^3}{\Theta_D^3} \int_0^{\omega_D} \frac{\hbar^5 \omega^4 e^{\frac{\hbar\omega}{k_B T}}}{k_B^5 T^5 \left(e^{\frac{\hbar\omega}{k_B T}} - 1\right)^2} d\omega. \tag{6}$$

In this relationship, $\hbar$ is the reduced Planck constant, k_B the Boltzmann constant, Θ_D the Debye temperature, and $N = \int_0^\infty D_p(\omega) d\omega$. Assuming all the phonons are involved in the high-temperature range, $N = \frac{4N_A}{\mathrm{M}}$ where $\mathrm{M} = 2\mathrm{M_{Cr}} + \mathrm{M_{Al}} + \mathrm{M_C}$ is the total molar mass. Using the Debye approximation, it comes to $N = \frac{V_0 \omega_D^3}{6\pi^3 v^3}$ where V_0 is the volume of the elementary cell. In addition, the Debye temperature $\Theta_D = \frac{\hbar\omega_D}{k_B} = \frac{\hbar(6N\pi^2 v^3)^{1/3}}{k_B}$ is found to be 675 K, which is the value frequently reported in the literature.[60] The heat capacity related to optical modes is estimated using the Einstein model as:

$$C_p^{ph}(\mathrm{OM}) = \frac{3 N k_B \Theta_E^2 e^{\frac{\Theta_E}{T}}}{T^2 (e^{\frac{\Theta_E}{T}} - 1)^2} \tag{7}$$

where $\Theta_E = \frac{\hbar\omega_E}{k_B}$ is the Einstein temperature. Finally, at high temperature, anharmonic effects can also be taken into account as a contribution to the heat capacity using:

$$C_p^{an} = \frac{9 N_A \alpha_V^2 B V_0 T}{M} \tag{8}$$

where B is the bulk modulus, and α_V the thermal expansion coefficient.

The total heat capacity distributed among its various contributions (electrons, phonons and anharmonic processes - thermal expansion) and computed using the data reported in Table I, is presented in Fig. 4(a) by a black line that overlaps the experimental results in blue.

2. Electronic thermal conductivity

Wiedemann-Franz law. As a first approximation, the electronic contribution to the thermal conductivity κ_e can be quickly estimated using the Wiedemann-Franz law as:

$$\kappa_e = \frac{L_0 T}{\rho(T)} \tag{9}$$

In this relationship, $L_0 = 2.45 \times 10^{-8}\mathrm{W\Omega K^{-2}}$ is the Lorentz number and $\rho(T)$ is the temperature-dependent electrical resistivity. The experimental in-plane electrical resistivity $\rho_{\parallel}(T)$ depicted in Fig. 3(a) is used to compute the in-plane electronic thermal conductivity $\kappa_e^{\parallel}$. As expected from the quasi-linear temperature-dependence of the resistivity, an almost temperature-independent electronic thermal conductivity is observed in Fig. 5(a).

Boltzmann transport equation. From first principles, the electronic contribution to the thermal conductivity κ_e can be obtained by solving the BTE for electrons. The BTE describes the statistical behavior of an out-of-equilibrium system in terms of various scattering processes considering their specific scattering rates. The transport distribution function is defined as:

$$\sigma(\varepsilon, T) = \int \sum_b \mathbf{v}_{b,\mathbf{k}} \times \mathbf{v}_{b,\mathbf{k}} \boldsymbol{\tau}_{b,\mathbf{k}} \delta\left(\varepsilon - \varepsilon_{b,\mathbf{k}}\right) \frac{d\mathbf{k}}{8\pi^3} \tag{10}$$

where b is a band index, $\mathbf{k}$ the conserved wavevector, $\mathbf{v}_{b,\mathbf{k}}$ the carrier velocities, $\boldsymbol{\tau}_{b,\mathbf{k}}$ the relaxation time, and $\varepsilon_{b,\mathbf{k}}$ the band energies. $\sigma(\varepsilon, T)$ can be used to compute the moments of the generalized transport coefficients:

$$\boldsymbol{\mathcal{L}}^{\boldsymbol{\alpha}} = q^2 \int \sigma(\varepsilon, T) \left(\varepsilon - \mu\right)^{\alpha} \left(-\frac{\partial f_F(\varepsilon; \mu, T)}{\partial \varepsilon}\right) d\varepsilon \tag{11}$$

with f_F the Fermi distribution and μ the chemical potential, that, in turn, are used to access the electronic transport coefficients of interest, namely the electrical conductivity σ, and the electronic thermal conductivity κ_e, as:

$$\sigma = \boldsymbol{\mathcal{L}}^{(\mathbf{0})} \tag{12}$$

$$\kappa_e = \frac{1}{q^2 T} \left[\frac{\left(\boldsymbol{\mathcal{L}}^{(\mathbf{1})}\right)^2}{\boldsymbol{\mathcal{L}}^{(\mathbf{0})}} - \boldsymbol{\mathcal{L}}^{(\mathbf{2})} \right]. \tag{13}$$

The integration of the BTE requires an accurate description of the electronic band structure. BoltzTraP2 code[30] provides such a description using an interpolation method based on a Fourier expansion that takes as input the electronic energies for different k-points, previously calculated by a DFT code [see Fig. 6(a)]. The code then computes the Fermi integrals for different temperatures and Fermi levels, and returns as output all the transport coefficients.[29,30] In this work, calculations are performed at zero-doping.

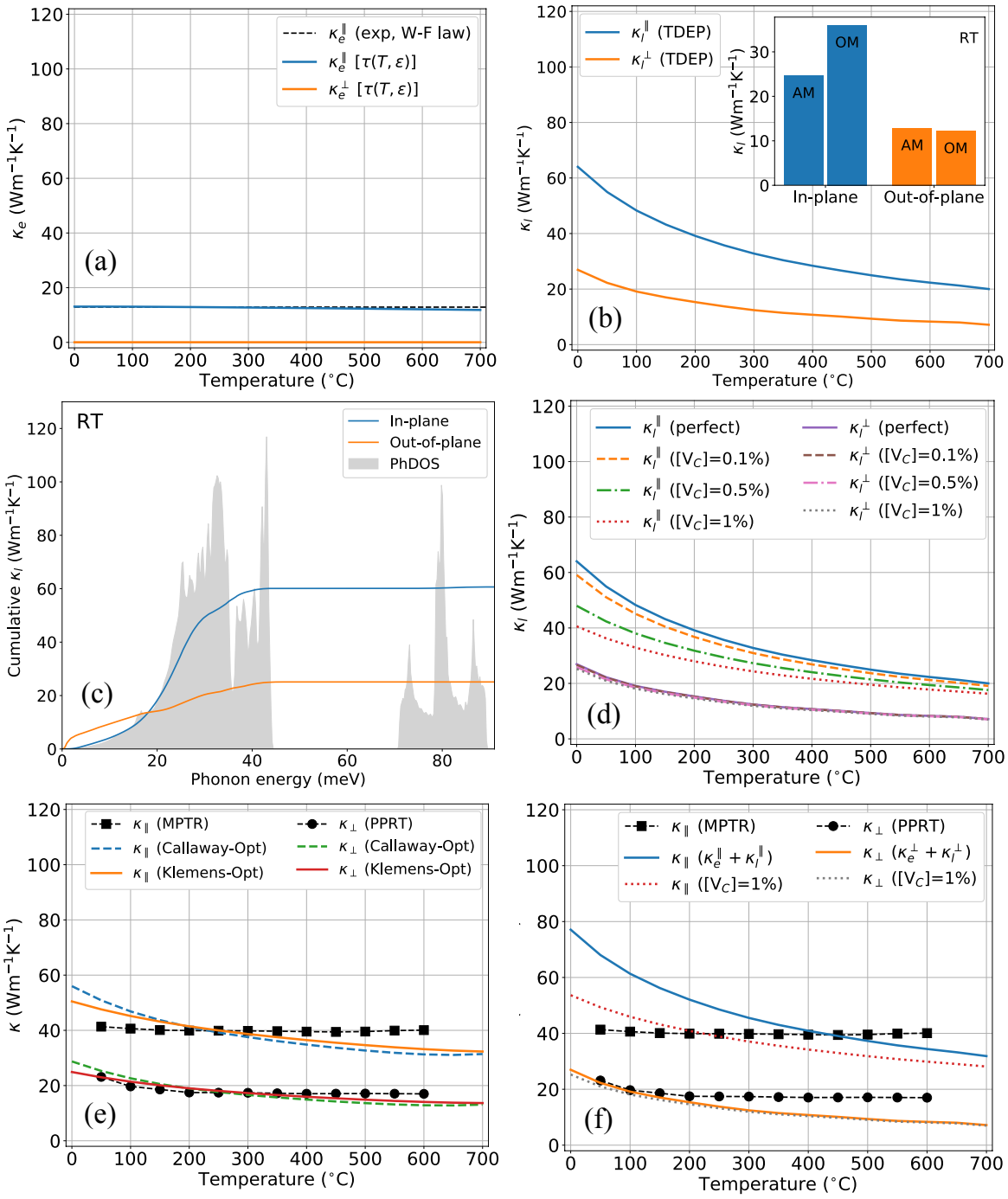

FIG. 5. (a) In-plane κ_e extracted from the Wiedemann-Franz law considering the experimental electrical resistivity $\rho_{\parallel}(T)$ from Fig. 3(a) and κ_e computed with $\tau(T,\varepsilon)$ defined in Eq. 15, (b) κ_l computed with anharmonic phonon-phonon scattering processes, with the contribution from optical and acoustic modes (OM and AM, respectively) at RT shown in the inset, (c) cumulative lattice thermal conductivity at RT, (d) κ_l for various concentrations of C vacancies, (e) κ obtained as the sum of κ_e and the predicted κ_l from Callaway and Klemens models, and (f) total computed thermal conductivity compared to the experimental curves obtained in this work.

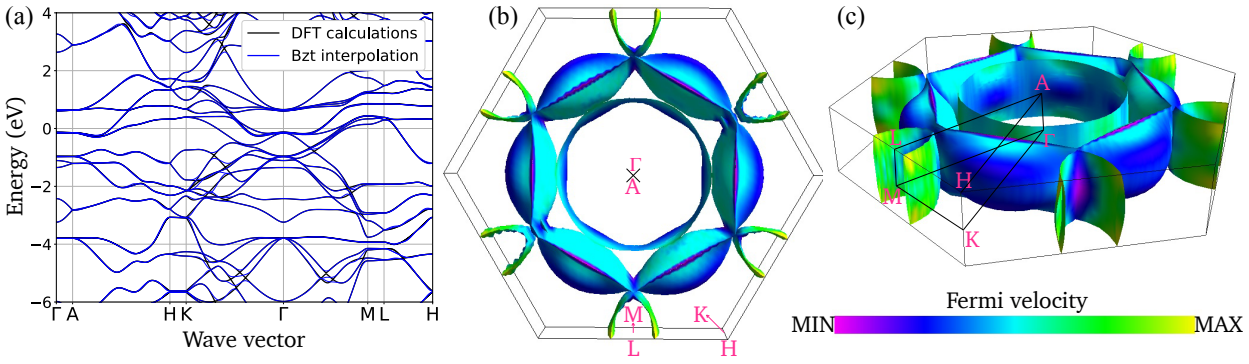

FIG. 6. First-principles (a) electronic band structure of Cr_2AlC, with the Fermi level fixed as the reference of zero energy, and (b) and (c) Fermi surfaces computed using the Fermisurfer code[50] and color-coded depending on Fermi velocities.

The relaxation time $\boldsymbol{\tau}_{b,\mathbf{k}}$ typically depends on the temperature T and on the charge carrier energy ε. All scattering events that can influence the electron conduction such as impurity scattering, phonon scattering, etc., are summed in this parameter according to the Matthiessen law.[62] In many cases, as a first approximation, the relaxation time is often assumed to be constant. Within the constant relaxation time approximation (CRTA), quantities such as $\sigma_0 = \sigma/\tau_0$ and $\kappa_0 = \kappa/\tau_0$ are determined by the band structure where the temperature dependence exclusively comes from the electronic occupation function. This approach is quite efficient in terms of computational time and globally provides good quantitative agreement with experimental measurements for lightly-doped semiconductors[63] where charge carriers are concentrated in specific bands and wave vectors. However, for highly-doped semiconductors and metals, charge carriers are located at various places (various bands b and wave vectors $\mathbf{k}$) and the electronic relaxation time thus varies significantly on the Fermi surface.[64] In these particular cases, the CRTA has shown limitations and more-advanced computational theories or models must be considered.

In order to obtain a good description of the electronic properties of metallic systems, both the temperature- and energy-dependence of $\boldsymbol{\tau}_{b,\mathbf{k}}$ must be considered in Eq. 10. The temperature and energy dependence is dictated by the scattering mechanisms. The most important mechanisms of electron scattering in metals are (i) defects and charged impurity scattering, dominant at low temperature ($< 100\,\mathrm{K}$), and (ii) electron-phonon scattering, dominant at high-temperature. An analytical model expression for $\tau\,(T, \varepsilon)$, developed on

the basis of known semi-classical theories can be formulated as:[65,66]

$$\tau\left(T,\varepsilon\right)=\tau_{\mathrm{ref}}\left(\frac{T}{T_{\mathrm{ref}}}\right)^{\gamma}\left(\frac{\varepsilon}{\varepsilon_{\mathrm{ref}}}\right)^{\lambda-1/2} \tag{14}$$

where τ_{ref} is a suitable reference value of τ at a temperature T_{ref} and $\varepsilon_{\mathrm{ref}}$ is the bottom of the conduction band. At low temperature, γ and λ exponents in Eq. 14 are respectively 0 and 2 reflecting the effect of defects and impurities. At high temperature, γ and λ exponents are respectively equal to -1 and 0 and the linear temperature dependence T^{-1} of the relaxation time reflects the dominance of electron-phonon scattering mechanisms. Given that we are interested in the $[0-700]$°C temperature range for which the relaxation time is governed by electron-phonon scattering processes, the expression of the relaxation time is given by:

$$\tau\left(T,\varepsilon\right)=\tau_{\mathrm{ref}}\left(\frac{T}{T_{\mathrm{ref}}}\right)^{-1}\left(\frac{\varepsilon}{\varepsilon_{\mathrm{ref}}}\right)^{-1/2} \tag{15}$$

where $\varepsilon_{\mathrm{ref}}$ is taken as the Fermi energy for a metallic system. The T^{-1} dependence in the model relaxation time allows to recover the linear temperature dependence of $\rho_{\parallel}(T)$ in Fig. 3(a). A value of $\tau_{\mathrm{ref}}=5\,\mathrm{fs}$ at $T_{\mathrm{ref}}=273\,\mathrm{K}$ is chosen to fit the experimental in-plane resistivity curve in Fig. 3(a), and is in good agreement with recently determined electronic relaxation times in Cr_2AlC single crystals.[67] Similarly, a value of $\tau_{\mathrm{ref}}=0.06\,\mathrm{fs}$ at $T_{\mathrm{ref}}=273\,\mathrm{K}$ is chosen to match the out-of-plane resistivity value of $1.5\times10^{-4}\,\Omega\mathrm{m}$ at 273 K [see Fig. 3(b)].[25] Since no experimental data is available for $\rho_{\perp}$ above 273 K, the only indication used to extract a physical relaxation time is the anisotropy ratio of ~ 300 observed for the resistivity at 273 K.[25] The temperature- and energy-dependent relaxation time has been implemented in the BoltzTraP2 code and is used to investigate the electrical and thermal transport in Cr_2AlC single crystals.

In Fig. 5(a), $\kappa_e^{\parallel}$ and $\kappa_e^{\perp}$ are reported using the temperature- and energy-dependent relaxation time defined in Eq. 15. A value of $13\,\mathrm{Wm^{-1}K^{-1}}$ ($0.04\,\mathrm{Wm^{-1}K^{-1}}$) at RT for the in-plane (out-of-plane) direction is obtained, and remains quasi-constant in the whole temperature range.

3. Lattice thermal conductivity

The lattice thermal conductivity κ_l of a perfect harmonic crystal is infinite and not a function of temperature. The lattice thermal resistance is dictated by phonon scattering

processes that can be intrinsic, through anharmonic phonon-phonon scattering, or extrinsic, induced by isotopic disorder, point defects, or edge effects. The treatment of these scattering processes is mandatory in order to obtain a good description and temperature-dependence of thermal and thermodynamic properties, especially at high temperature.

Phonon Boltzmann transport equation. When a material is at equilibrium at the temperature T, the equilibrium phonon population $\overline{n}_\nu$ describes the number of phonons for each vibrational mode ν found at energy $\hbar\omega_\nu$. If a gradient of temperature is applied, the phonon population deviates from its equilibrium condition and reaches an out-of-equilibrium condition.[68]

The first microscopic description of the lattice thermal conductivity was formulated in 1929 by Peierls,[69] and is nowadays known as the phonon BTE. This equation describes how the perturbation due to a gradient of temperature involves a change in the phonon population due to all possible scattering mechanisms. In order to accurately predict thermal transport properties, an accurate description of the equilibrium and perturbed phonon populations is required, as well as of their interactions, and lifetimes.[68] In practice, the harmonic quantities, such as phonon frequencies, group velocities, and phonon populations, can be obtained *ab initio* by computing the second-order IFC using DFPT. The challenge thus resides in the determination of the anharmonic quantities, such as phonon scattering rates and linewidths. The total out-of-equilibrium distribution n_ν in its linearized form is given by:

$$n_\nu = \overline{n}_\nu \left(\overline{n}_\nu + 1\right) F_\nu \nabla T \tag{16}$$

where F_ν corresponds to the deviation of the phonon population with respect to the equilibrium condition. The computation of n_ν, which is the key quantity to be evaluated, requires to solve the linearized BTE for phonons:

$$c_\nu \nabla T \frac{\partial \overline{n}_\nu}{\partial T} = \sum_{\nu'} \Omega_{\nu,\nu'} n_{\nu'} \tag{17}$$

where $\Omega_{\nu,\nu'}$ is a matrix of scattering rates acting on the phonon population. The lattice thermal conductivity can be expressed as:

$$\kappa_l = \frac{\hbar^2}{\Omega k_B T^2} \sum_\nu \overline{n}_\nu \left(\overline{n}_\nu + 1\right) c_\nu \omega_\nu F_\nu \tag{18}$$

where Ω is the unit cell volume, ω_ν the phonon frequencies, and c_ν the corresponding group velocities. Additional information on the computation of the lattice thermal conductivity can be found in Ref.[68].

In most cases, phonons are treated individually through the single mode approximation (SMA).[70–72] This relies on the assumption that heat-current is dissipated every time a phonon undergoes a scattering event,[73] and approximates F_ν with $c_\nu\omega_\nu\tau_\nu$ where τ_ν is the relaxation time of the phonon mode ν. While the SMA properly describes the depopulation of a phonon mode after any scattering process, the repopulation process is usually poorly described due to a loss of memory of the initial phonon distribution (final states are repopulated isothermally).[73,74] In particular, the SMA has shown some limitations to accurately describe the lattice thermal conductivity in layered compounds and two-dimensional systems.[73]

Recently, Hellman *et al.*[31–33] proposed a formalism to obtain the third-order IFCs and to accurately calculate the lattice thermal conductivity from the iterative solution of the phonon BTE. The first step consists in computing the second- and third-order force constant matrices that are both temperature- and volume-dependent. For this purpose, an ensemble of 30 non-correlated configurations generated from a gaussian distribution of harmonic input phonons is used to sample the Born-Oppenheimer potential energy surface at finite temperature. Then, a minimization scheme between the forces model and the *ab initio* computed forces is used, and leads to the direct determination of the force constant matrices. The second step consists in iteratively solving the phonon Boltzmann equation in Eq. 18, starting from an initial guess F_ν^0 to obtain the non-equilibrium distribution.

Figure 5(b) presents the computed lattice thermal conductivities in-plane $\kappa_l^{\parallel}$ and out-of-plane $\kappa_l^{\perp}$ for Cr_2AlC single crystals, when only anharmonic phonon-phonon scattering processes are considered. The inclusion of isotopic scattering processes does not modify the lattice thermal conductivity, as expected from the small natural isotopic diversity of Cr, Al, and C elements. Grain boundary scattering processes can play an important role in phonon transport as polycrystallinity tends to drastically decrease the lattice thermal conductivity.[75] However, in the present work, there is no reason to include these scattering processes since all measurements are performed on single crystals with a single grain of a few cm^2. Phonon scattering from point defects can also play an important role in limiting the thermal conductivity. Since both experimental and theoretical works gave evidence for

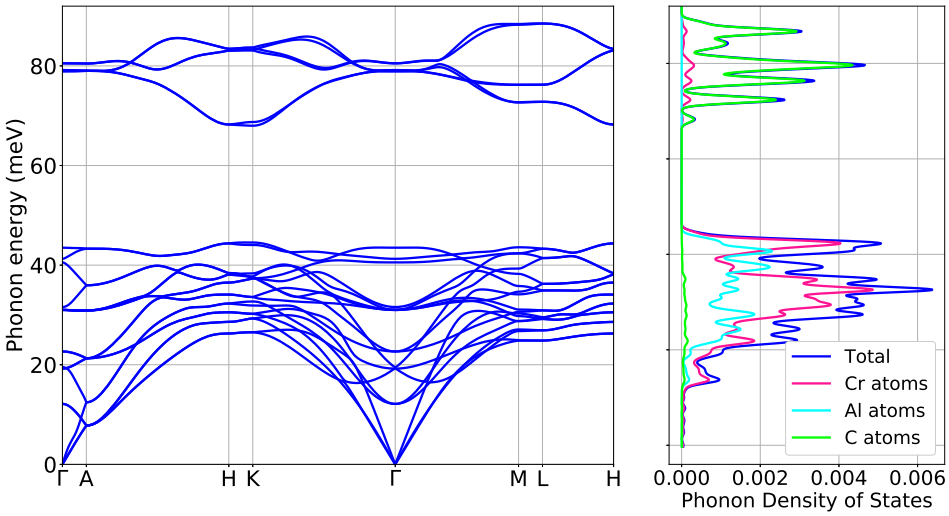

FIG. 7. First-principles phonon spectrum of Cr_2AlC along major crystallographic directions with the projected phonon density of states.[28]

significant amounts of vacancies in MAX phases,[2,76] these defects are taken into account in the computation of the lattice thermal conductivity. A vacancy can be regarded as a perturbation of the crystal corresponding to the removal of the mass of one atom and the force constants of two atoms.[77] Hence, the energy associated to a vacancy can be treated as equivalent to an isotopic defect corresponding to a change of mass $\Delta M = -3M$ where M is the atomic mass of the missing atom,[77] *i.e.*, C atom in Cr_2AlC.[76] Concentrations of C vacancies ranging from 0.1% to 1% are considered. The results are presented in Fig. 5(d). While $\kappa_l^{\perp}$ remains almost constant over the whole temperature range, $\kappa_l^{\parallel}$ is reduced, especially in the $[0-300]$°C temperature range by the inclusion of C vacancies. This can be understood from the analysis of the high-energy phonon branches in Fig. 7 and detailed in Ref.[28]. In fact, the presence or absence of C atoms only affects the in-plane phonon propagation and lattice thermal conductivity since, for the high-energy C-related modes, there is no phonon propagation feasible perpendicularly to the plane, due to the flatness of the bands.

Callaway and Klemens models. An efficient alternative to the phonon BTE to compute the lattice thermal conductivity is the Debye-Callaway model (detailed in appendix 1). Considering the optimized values for the parameters used in the model, both the in-plane and the out-of-plane lattice thermal conductivities are computed and the total thermal con-

ductivities, including the electronic contributions, are presented (dashed lines) in Fig. 5(e). The agreement for both $\kappa_{\parallel}$ and $\kappa_{\perp}$ with the experimental curves is quite good.

Using the Klemens model (detailed in appendix 2) and optimizing at the same time both the effects of umklapp processes and defects lead to the curves (solid lines) presented in Fig. 5(e). The agreement with the experimental curves is good and is slightly improved with respect to the Callaway model, especially around RT.

IV. DISCUSSION

In Fig. 4(a), the experimental measurements of the heat capacity of Cr_2AlC are slightly different from the values reported by Tian *et al.*[53] However, the theoretical total heat capacity reproduces the experimental data with very good accuracy, inducing a high confidence in the measurement techniques used. In addition, such agreement allows us to state that the AM contribution is clearly the dominant one, while the electronic, anharmonic, and OM contributions are similar in magnitude and remain low compared to the AM contribution.

A linear temperature-dependence for the electrical resistivity is observed in Fig. 3(a), as is usual in metals, due to the linear increase of the phonon occupation with temperature. Not surprisingly, the Wiedemann-Franz law gives a good approximation of the electronic thermal conductivity, and leads to results similar to those obtained with the BoltzTraP2 code using a temperature-dependent relaxation time [see Fig. 5(a)]. The large anisotropy observed in the electrical resistivities,[25] with an out-of-plane resistivity about 300 times higher than the in-plane one, leads to a negligible electronic contribution to the out-of-plane thermal conductivity. This anisotropy in the electronic transport can also be noticed from the electronic band structure and Fermi surface in Fig. 6. The open tubular structure of the Fermi surface depicted in Figs. 6(b) and 6(c) suggests a quasi two-dimensional character of the Cr_2AlC system, in agreement with results from Ito *et al.*[27] Moreover, from Eq. 10, it is clear that carrier velocities, which are linked to the band dispersion, play an important role in the electronic transport. As a consequence, in Fig. 6(a), the dispersive bands along directions parallel to the plane (*i.e.*, A−H, Γ−K, Γ−M, L−H) will lead to high carrier velocities and good electronic conductivity in the plane, while the almost flat bands along directions perpendicular to the plane (*i.e.*, Γ−A, H−K, M−L) explain the weak out-of-plane

conductivity. This is confirmed by the evaluation of the carrier velocities at the Fermi surface [see Figs. 6(b) and 6(c)] for which the in-plane component is higher than the out-of-plane one (not shown).

The results for the lattice thermal conductivity computed with the TDEP code, considering anharmonic phonon-phonon scattering processes, are shown in Fig. 5(b). Both in-plane and out-of-plane κ_l decrease with the temperature, which is a signature of umklapp-dominated scattering processes. Although Cr_2AlC has relatively isotropic sound velocities [see Table I],[28] it has a significantly anisotropic lattice thermal conductivity. This can be explained from the cumulative κ_l depicted in Fig. 5(c) where the anisotropy clearly starts at energies greater than 20 meV, mostly corresponding to optical modes. The low-lying optical branches - with energy below 40 meV - in the phonon spectrum of Cr_2AlC [see Fig. 7] are very dispersive, with higher group velocities in the ab-plane (along $\Gamma-$K and $\Gamma-$M) than along the c-axis (along $\Gamma-$A). Consequently, the optical modes significantly contribute to κ_l, particularly for the in-plane direction as shown in the inset of Fig. 5(b). This decomposition partly explains the intrinsic anisotropy present in the MAX phases, in general, and in Cr_2AlC, in particular. A good qualitative and quantitative agreement with the experimental thermal conductivity can be reached by considering both Callaway and Klemens models for the computation of κ_l, with optimized parameters, as highlighted in Fig. 5(e).

The computed total thermal conductivities are presented in Fig. 5(f) and both slightly decrease with the temperature. An anisotropy ratio slightly higher than 2 is predicted over the whole temperature range. A comparison with the experimental data is also provided in Fig. 5(f). A qualitative agreement is found between experimental and computed thermal conductivity curves, with an overestimation of the experimental $\kappa_{\parallel}$ by 65% and an underestimation of the experimental $\kappa_{\perp}$ by 4% at 50°C. The overestimation of $\kappa_{\parallel}$ can be due to various electron/phonon scattering sources and intrinsic structural defects present in the samples and not considered in the calculations. For example, it was shown in Fig. 5(d) that the inclusion of C vacancies in our model reduces $\kappa_l^{\parallel}$ in the $[0-300]$°C temperature range, while keeping $\kappa_l^{\perp}$ constant. Consequently, the deviation between the calculated and experimental in-plane thermal conductivities at 50°C goes down to 55% and 19% considering scattering processes with C vacancies, with a concentration of 0.1 and 1%, respectively. This confirms that the overestimation of the in-plane thermal conductivity can be explained by missing scattering processes in the calculations, which can play an important role especially

around RT.

Interestingly, while the calculations predict a decreasing behavior for the thermal conductivity with the temperature - as intuitively deduced from the decrease of the phonon lifetimes with T - the experimental curves exhibit two different trends. For the in-plane thermal conductivity, some curves are decreasing with T while others are increasing with T, leading to an average curve which is almost constant on the whole temperature range. For the out-of-plane thermal conductivity, the curve slightly decreases before saturating above 200°C. It seems that something, which is not caught by our simulations, is maintaining the thermal current constant even at higher temperature. This could be linked to a possible thermal expansion with increasing T or with a potential annealing of the sample at higher T, reducing the number of defects in it. More work is needed to clarify this situation which will be the scope of our future research.

In the present work, the main result is the quantitative analysis of the anisotropy in the thermal conductivity of Cr_2AlC single crystals confirmed by both experimental and theoretical approaches. This anisotropy arises from both the electronic and lattice contributions; the latter being the dominant term. At RT, the lattice contribution represents $\sim 81\%$ of the total in-plane thermal conductivity, and decreases with T to reach 63% at 600°C. For the out-of-plane thermal conductivity, the electronic contribution is almost zero and the thermal transport is only feasible through lattice vibrations. Interestingly, the anisotropy ratio of 300 observed in the electronic transport is now reduced down to ~ 2 for the thermal transport, as a consequence of lattice vibrations which play an important role along both in-plane and out-of-plane directions.

V. CONCLUSIONS

In summary, the heat capacity of Cr_2AlC single crystals is measured and accurately reproduced using simple analytic models. The contribution from acoustic phonon modes is clearly the dominant one, while the electronic, anharmonic and optical modes contributions represent together at most 25% of the heat capacity.

The in-plane and out-of-plane thermal conductivities of Cr_2AlC single crystals are measured using various experimental techniques and compared to *ab initio* calculations. An

accurate microscopic description of heat transport is achieved and the electronic contribution to thermal conductivity is determined using a temperature-dependent electronic relaxation time. Solving iteratively the BTE for phonons, the lattice thermal conductivity is estimated. Additionally, Callaway and Klemens models provide a qualitative and quantitative description of the lattice thermal conductivity. Both in-plane and out-of-plane thermal conductivities computed *ab initio* are in good agreement with present experiments and with previously reported experimental data. For the out-of-plane thermal conductivity, the quantitative agreement is also correct in the entire temperature range. Regarding the in-plane thermal conductivity, the computed data slightly overestimate the experimental ones below 400°C, whereas they underestimate them at higher temperatures. The inclusion of scattering processes by C vacancies improves the prediction of $\kappa_{\parallel}$, especially between RT and 300°C, and leads to a good quantitative agreement with the experimental curve. The remaining deviation between calculated and experimental thermal conductivities can possibly be assigned to additional scattering phenomena, present in real samples, and not considered in this work. Besides, the saturating behavior of the experimental curves at high temperature is not caught by our simulations. It could be linked to a possible thermal expansion or annealing of the sample with increasing T. More investigation is needed to shed light on this interesting point.

As a main conclusion, the anisotropy reported experimentally is accurately reproduced theoretically and seems to mainly arise from the lattice contribution. A similar anisotropy in the transport properties is expected for other MAX phases with identical layered structures. Consequently, we believe that this first-principles approach can be effectively applied to investigate thermal conductivities of other layered systems. From an applicative aspect, accurately predicting and describing the anisotropic thermal conductivity in layered systems is essential for device engineering, especially for energy dissipation in electronics and high-temperature applications.

APPENDIX: LATTICE THERMAL CONDUCTIVITY MODELS

1. Callaway model

In the Debye-Callaway model, the lattice thermal conductivity is composed of two terms such that:[71]

$$\kappa_l = \kappa_1 + \kappa_2 \tag{19}$$

with

$$\kappa_1 = \frac{k_B^4}{2\pi^2 v\hbar^3} T^3 \int_0^{\Theta_D/T} \frac{x^4 e^x}{\left(e^x-1\right)^2} \tau_c dx \tag{20}$$

and

$$\kappa_2 = \frac{k_B^4}{2\pi^2 v\hbar^3} T^3 \frac{\left[\int_0^{\Theta_D/T} \frac{x^4 e^x}{(e^x-1)^2} \frac{\tau_c}{\tau_N} dx\right]^2}{\int_0^{\Theta_D/T} \frac{x^4 e^x}{(e^x-1)^2} \frac{\tau_c}{\tau_N \tau_q} dx} \tag{21}$$

with $x = \frac{\hbar\omega}{k_B T}$, and $\tau_c^{-1} = \tau_N^{-1} + \tau_q^{-1} = \tau_N^{-1} + \tau_B^{-1} + \tau_I^{-1} + \tau_U^{-1}$ the total relaxation time, where τ_N, τ_B, τ_I, and τ_U respectively correspond to the relaxation times associated to normal modes, grain boundary, point defect, and umklapp scattering processes. The relaxation time associated to normal modes is defined as $\tau_N^{-1} = A\omega^2 T = A\frac{x^2 k_B^2}{\hbar^2} T^3$. The relaxation time corresponding to the phonon scattering by grain boundary is defined as $\tau_B^{-1} = \frac{v}{L}$ with L the characteristic dimension of the crystal grain. The relaxation time for phonon scattering by point defects is given by $\tau_I^{-1} = C\omega^4 = C\frac{x^4 k_B^4 T^4}{\hbar^4}$ where the constant $C = \frac{V_0 \Gamma}{4\pi v^3}$ depends on the sound velocity v, the volume of the elementary cell V_0, and the mass defect parameter $\Gamma = \sum_i f_i \left(1 - \frac{M_i}{M}\right)^2$, with f_i the mass fraction of impurity for atom i with mass M_i. Eventually, the relaxation time associated to umklapp processes is defined by $\tau_U^{-1} = B\omega^2 T e^{-\frac{\Theta_D}{3T}} = B\frac{x^2 k_B^2}{\hbar^2} T^3 e^{-\frac{\Theta_D}{3T}}$, where $B = \frac{G^2 \hbar}{M_a v^2 \Theta_D}$ is a constant, with G the Grüneisen parameter, M_a the mass per atom, and v the sound velocity. At high temperature, for a significant level of impurities, all phonon modes are scattered by resistive processes and, hence, $\tau_N \gg \tau_q$ and $\tau_c \approx \tau_q$. As a consequence, $\kappa_1 \gg \kappa_2$ and the lattice thermal conductivity is given by the expression in Eq. 20.

Considering that phonons are mostly scattered by umklapp processes (τ_U) and point defects (τ_I) in the temperature range of interest, and using the computed values for both parameters B and C reported in Table II, an estimation of the in-plane and out-of-plane lattice thermal conductivities is obtained and reported in Figs. 8(a) and 8(b). Since both parameters cannot be identified independently, only the B parameter related to umklapp

TABLE II. Theoretical and optimized values of the parameters involved in Callaway and Klemens models.

	Callaway model			Klemens model	
	C	B	B_{opt}	K	K_{opt}
$\kappa_{\parallel}$	1.584×10^{-41}	3.011×10^{-19}	1.372×10^{-20}	151	620
$\kappa_{\perp}$			3.061×10^{-20}		412

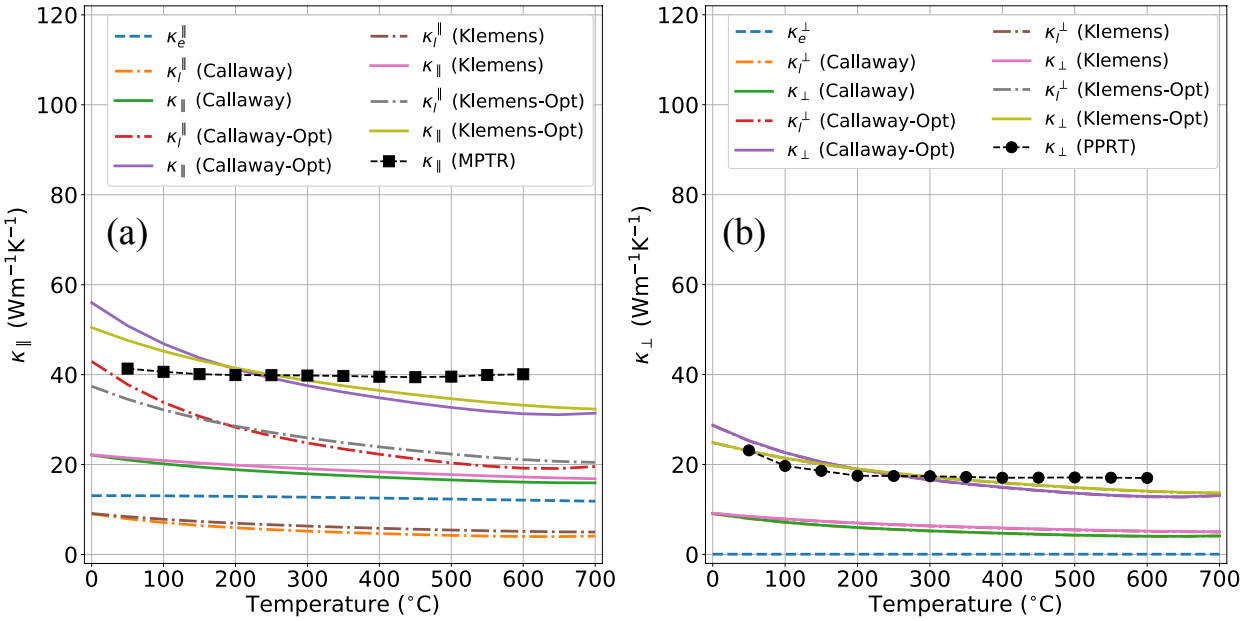

FIG. 8. (a) In-plane and (b) out-of-plane κ predicted from Callaway and Klemens models, compared to experimental measurements obtained in this work.

processes is optimized using the Levenberg-Marquardt algorithm. The values for B_{opt} in-plane and out-of-plane are reported in Table II and used to compute $\kappa_l^{\parallel}$ and $\kappa_l^{\perp}$, respectively.

2. Klemens model

The Klemens model assumes that both umklapp processes and defects play an important role in the high-temperature range. The lattice thermal conductivity is given by:

$$\kappa_{\infty,U,D} = \frac{k_b \pi}{4\pi^2 v \sqrt{CB}} \frac{1}{\sqrt{T}} = K \frac{1}{\sqrt{T}} \tag{22}$$

with the parameters B and C defined previously. The theoretical value of K is reported in Table II and is initally considered equal for both the in-plane and out-of-plane lattice thermal conductivities. Using the identical minimization process, optimized values for K are obtained. The results for the thermal conductivity in the Klemens approximation are shown in Figs. 8(a) and 8(b).

ACKNOWLEDGMENTS

A.C and J.-C.C. acknowledge financial support from the Fédération Wallonie-Bruxelles through the Action de Recherche Concertée (ARC) on 3D nanoarchitecturing of 2D crystals (No. 16/21-077), from the European Union's Horizon 2020 researchers and innovation program (Graphene Flagship Core 2 - No. 785219 and Core 3 No. 881603), and from the Belgium FNRS. A.C. acknowledges the support of Wallonie-Bruxelles-International. M.J.V. and J.-C.C. acknowledge PDR grant T.1077.15-1/7 from Belgain FNRS. T.O. was financially supported by the "Agence Nationale de la Recherche" (project ANR-18-CE09-0041). A.C., J.-C.C, and T.O. are also indebted to the Flag-ERA JTC 2017 project entitled "MORE-MXenes". M.W.B. acknowledges the financial support of the chair of excellence program of the Nanosciences Foundation (Université Grenoble-Alpes Foundation). This publication is also based upon work of the MELODICA project, funded by the EU Flag-ETA JTC 2017 call. Computational resources were provided by the supercomputing facilities of the UCLouvain (CISM) and the Consortium des Equipements de Calcul Intensif en Fédération Wallonie-Bruxelles (CECI) funded by the Fonds de la Recherche Scientifique de Belgique (F.R.S.- FNRS) under convention No. 2.5020.11. A.C. thanks M. Giantomassi, G. Petretto, and X. Gonze for discussions and ideas shared together.

---

* aurelie.champagne@uclouvain.be

REFERENCES

[1] Michel W. Barsoum, "The mn+1axn phases: A new class of solids: Thermodynamically stable nanolaminates," Progress in Solid State Chemistry **28**, 201 – 281 (2000).

[2] Maxim Sokol, Varun Natu, Sankalp Kota, and Michel W. Barsoum, "On the chemical diversity of the max phases," Trends in Chemistry **1**, 210 – 223 (2019).

[3] Zhimou Liu, Erdong Wu, Jiemin Wang, Yuhai Qian, Huimin Xiang, Xichao Li, Qianqian Jin, Guangai Sun, Xiping Chen, Jingyang Wang, and Meishuan Li, "Crystal structure and formation mechanism of (cr2/3ti1/3)3alc2 max phase," Acta Materialia **73**, 186 – 193 (2014).

[4] Quanzheng Tao, Martin Dahlqvist, Jun Lu, Sankalp Kota, Rahele Meshkian, Joseph Halim, Justinas Palisaitis, Lars Hultman, Michel W. Barsoum, Per O.Å. Persson, and Johanna Rosen, "Two-dimensional Mo1.33C MXene with divacancy ordering prepared from parent 3D laminate with in-plane chemical ordering," Nature Communications **8**, 1–7 (2017).

[5] Martin Dahlqvist, Jun Lu, Rahele Meshkian, Quanzheng Tao, Lars Hultman, and Johanna Rosen, "Prediction and synthesis of a family of atomic laminate phases with kagomé-like and in-plane chemical ordering," Science Advances **3**, 1 – 9 (2017).

[6] Q. Tao, T. Ouisse, D. Pinek, O. Chaix-Pluchery, F. Wilhelm, A. Rogalev, C. Opagiste, L. Joufret, A. Champagne, J.-C. Charlier, J. Lu, L. Hultman, M. W. Barsoum, and J. Rosen, "Rare-earth (re) nanolaminates $mo_4re_4al_7c_3$ featuring ferromagnetism and mixed-valence states," Phys. Rev. Materials **2**, 114401 (2018).

[7] Quanzheng Tao, Jun Lu, Martin Dahlqvist, Aurelija Mockute, Stuart Calder, Andrejs Petruhins, Rahele Meshkian, Oleg Rivin, Daniel Potashnikov, El'ad Caspi, Hagai Shaked, Andreas Hoser, Christine Opagiste, Rose-Marie Galera, Ruslan Salikhov, Ulf Wiedwald, Clemens Ritter, Andrew R. Wildes, Brje Johansson, Lars Hultman, Michael Farle, Michel W. Barsoum, and Johanna Rosen, "Atomically layered and ordered rare-earth i-max phases: A new class of magnetic quaternary compounds," Chemistry of Materials **31**, 2476–2485 (2019).

[8] Andrejs Petruhins, Jun Lu, Lars Hultman, and Johanna Rosen, "Synthesis of atomically layered and chemically ordered rare-earth (re) i-max phases; (mo2/3re1/3)2gac with re = gd, tb, dy, ho, er, tm, yb, and lu," Materials Research Letters **7**, 446–452 (2019).

[9] Michel W. Barsoum, *MAX Phases*, 1st ed. (Wiley-Blackwell, 2013).

[10] M. W. Barsoum and T. El-Raghy, "The MAX Phases: Unique New Carbide and Nitride Materials," American Scientist **89**, 334 (2001).

[11] Matt Nelson, Matthias T. Agne, Babak Anasori, Jian Yang, and Michel W. Barsoum, "Synthesis and characterization of the mechanical properties of ti3sic2/mg and cr2alc/mg alloy composites," Materials Science and Engineering: A **705**, 182 – 188 (2017).

[12] Jacob Gruber, Andrew C. Lang, Justin Griggs, Mitra L. Taheri, Garritt J. Tucker, and Michel W. Barsoum, "Evidence for bulk ripplocations in layered solids," Scientific Reports **6**, 33451 (2016).

[13] Justin Griggs, Andrew C. Lang, J. Gruber, G.J. Tucker, M.L. Taheri, and M.W. Barsoum, "Spherical nanoindentation, modeling and transmission electron microscopy evidence for ripplocations in ti3sic2," Acta Materialia **131**, 141 – 155 (2017).

[14] M.W. Barsoum and G.J. Tucker, "Deformation of layered solids: Ripplocations not basal dislocations," Scripta Materialia **139**, 166 – 172 (2017).

[15] M. W. Barsoum, X. Zhao, S. Shanazarov, A. Romanchuk, S. Koumlis, S. J. Pagano, L. Lamberson, and G. J. Tucker, "Ripplocations: A universal deformation mechanism in layered solids," Phys. Rev. Materials **3**, 013602 (2019).

[16] Hussein O. Badr, Aurélie Champagne, Thierry Ouisse, Jean-Christophe Charlier, and Michel W. Barsoum, "Elastic properties and hardness values of v_2AlC and Cr_2AlC single crystals," Phys. Rev. Materials **4**, 083605 (2020).

[17] Michael Naguib, Murat Kurtoglu, Volker Presser, Jun Lu, Junjie Niu, Min Heon, Lars Hultman, Yury Gogotsi, and Michel W. Barsoum, "Two-dimensional nanocrystals produced by exfoliation of Ti3AlC2," Advanced Materials **23**, 4248–4253 (2011).

[18] Michel W. Barsoum and Tamer El-Raghy, "Synthesis and characterization of a remarkable ceramic: Ti3sic2," Journal of the American Ceramic Society **79**, 1953–1956 (1996).

[19] Monika K. Drulis, H. Drulis, S. Gupta, M. W. Barsoum, and T. El-Raghy, "On the heat capacities of m2alc (m=ti,v,cr) ternary carbides," Journal of Applied Physics **99**, 093502 (2006).

[20] J. D. Hettinger, S. E. Lofland, P. Finkel, T. Meehan, J. Palma, K. Harrell, S. Gupta, A. Ganguly, T. El-Raghy, and M. W. Barsoum, "Electrical transport, thermal transport, and elastic properties of M_2AlC (m = Ti, cr, nb, and v)," Phys. Rev. B **72**, 115120 (2005).

[21] F. Mercier, T. Ouisse, and D. Chaussende, "Morphological instabilities induced by foreign particles and ehrlich-schwoebel effect during the two-dimensional growth of crystalline ti_3sic_2," Phys. Rev. B **83**, 075411 (2011).

[22] Frdric Mercier, Odette Chaix-Pluchery, Thierry Ouisse, and Didier Chaussende, "Raman scattering from ti3sic2 single crystals," Applied Physics Letters **98**, 081912 (2011).

[23] T. Ouisse, E. Sarigiannidou, O. Chaix-Pluchery, H. Roussel, B. Doisneau, and D. Chaussende, "High temperature solution growth and characterization of Cr_2AlC single crystals," Journal of

Crystal Growth **384**, 88–95 (2013).

[24] L. Shi, T. Ouisse, E. Sarigiannidou, O. Chaix-Pluchery, H. Roussel, D. Chaussende, and B. Hackens, "Synthesis of single crystals of v2alc phase by high-temperature solution growth and slow cooling technique," Acta Materialia **83**, 304 – 309 (2015).

[25] T. Ouisse, L. Shi, B. A. Piot, B. Hackens, V. Mauchamp, and D. Chaussende, "Magnetotransport properties of nearly-free electrons in two-dimensional hexagonal metals and application to the $M_{n+1}aX_n$ phases," Phys. Rev. B **92**, 045133 (2015).

[26] Thierry Ouisse and Michel W. Barsoum, "Magnetotransport in the max phases and their 2d derivatives: Mxenes," Materials Research Letters **5**, 365–378 (2017).

[27] Takahiro Ito, Damir Pinek, Taishi Fujita, Masashi Nakatake, Shin-ichiro Ideta, Kiyohisa Tanaka, and Thierry Ouisse, "Electronic structure of Cr_2AlC as observed by angle-resolved photoemission spectroscopy," Phys. Rev. B **96**, 195168 (2017).

[28] A. Champagne, F. Bourdarot, P. Bourges, P. Piekarz, D. Pinek, I. Glard, J.-C. Charlier, and T. Ouisse, "Phonon dispersion curves in cr2alc single-crystals," Materials Research Letters **6**, 378–383 (2018).

[29] Georg K.H. Madsen and David J Singh, "BoltzTraP. A code for calculating band-structure dependent quantities," Computer Physics Communications **175**, 67–71 (2006).

[30] Georg K.H. Madsen, Jesús Carrete, and Matthieu J. Verstraete, "BoltzTraP2, a program for interpolating band structures and calculating semi-classical transport coefficients," Computer Physics Communications **231**, 140–145 (2018).

[31] O. Hellman, I. A. Abrikosov, and S. I. Simak, "Lattice dynamics of anharmonic solids from first principles," Phys. Rev. B **84**, 180301 (2011).

[32] Olle Hellman, Peter Steneteg, I. A. Abrikosov, and S. I. Simak, "Temperature dependent effective potential method for accurate free energy calculations of solids," Phys. Rev. B **87**, 104111 (2013).

[33] Olle Hellman and I. A. Abrikosov, "Temperature-dependent effective third-order interatomic force constants from first principles," Phys. Rev. B **88**, 144301 (2013).

[34] L. J. Swartzendruber, "Correction factor tables for four-point probe resistivity measurements on thin, circular semiconductor samples," Technical note **6**, 43 (1964).

[35] Andrzej Kusiak, Jiri Martan, Jean-Luc Battaglia, and Rostislav Daniel, "Using pulsed and modulated photothermal radiometry to measure the thermal conductivity of thin films," Ther-

mochimica Acta **556**, 1 – 5 (2013).

[36] L. Gaverina, J. C. Batsale, A. Sommier, and C. Pradere, "Pulsed flying spot with the logarithmic parabolas method for the estimation of in-plane thermal diffusivity fields on heterogeneous and anisotropic materials," Journal of Applied Physics **121**, 115105 (2017).

[37] Emmanuel Ruffio, Christophe Pradere, Alain Sommier, Jean-Christophe Batsale, Andrzej Kusiak, and Jean-Luc Battaglia, "Signal noise ratio improvement technique for bulk thermal diffusivity measurement," International Journal of Thermal Sciences **129**, 385 – 395 (2018).

[38] P. Hohenberg and W. Kohn, "Inhomogeneous electron gas," Phys. Rev. **136**, B864–B871 (1964).

[39] W. Kohn and L. J. Sham, "Self-consistent equations including exchange and correlation effects," Phys. Rev. **140**, A1133–A1138 (1965).

[40] Stefano Baroni, Paolo Giannozzi, and Andrea Testa, "Green's-function approach to linear response in solids," Phys. Rev. Lett. **58**, 1861–1864 (1987).

[41] Xavier Gonze, "Perturbation expansion of variational principles at arbitrary order," Phys. Rev. A **52**, 1086–1095 (1995).

[42] Xavier Gonze, "First-principles responses of solids to atomic displacements and homogeneous electric fields: Implementation of a conjugate-gradient algorithm," Phys. Rev. B **55**, 10337–10354 (1997).

[43] Xavier Gonze and Changyol Lee, "Dynamical matrices, born effective charges, dielectric permittivity tensors, and interatomic force constants from density-functional perturbation theory," Phys. Rev. B **55**, 10355–10368 (1997).

[44] Stefano Baroni, Stefano de Gironcoli, Andrea Dal Corso, and Paolo Giannozzi, "Phonons and related crystal properties from density-functional perturbation theory," Rev. Mod. Phys. **73**, 515–562 (2001).

[45] X. Gonze, J.-M. Beuken, R. Caracas, F. Detraux, M. Fuchs, G.-M. Rignanese, L. Sindic, M. Verstraete, G. Zerah, F. Jollet, M. Torrent, A. Roy, M. Mikami, Ph. Ghosez, J.-Y. Raty, and D.C. Allan, "First-principles computation of material properties: the {ABINIT} software project," Computational Materials Science **25**, 478 – 492 (2002).

[46] X Gonze, G Rignanese, M Verstraete, J Betiken, Y Pouillon, R Caracas, F Jollet, M Torrent, G Zerah, M Mikami, P Ghosez, M Veithen, J-Y Raty, V Olevano, F Bruneval, L Reining, R Godby, G Onida, D Hamann, and D Allan, "A brief introduction to the abinit software package," Zeitschrift für Kristallographie (Special number on Computational Crystallography)

220, 558–562 (2005).

[47] X. Gonze, B. Amadon, P.-M. Anglade, J.-M. Beuken, F. Bottin, P. Boulanger, F. Bruneval, D. Caliste, R. Caracas, M. Ct, T. Deutsch, L. Genovese, Ph. Ghosez, M. Giantomassi, S. Goedecker, D.R. Hamann, P. Hermet, F. Jollet, G. Jomard, S. Leroux, M. Mancini, S. Mazevet, M.J.T. Oliveira, G. Onida, Y. Pouillon, T. Rangel, G.-M. Rignanese, D. Sangalli, R. Shaltaf, M. Torrent, M.J. Verstraete, G. Zerah, and J.W. Zwanziger, "Abinit: First-principles approach to material and nanosystem properties," Computer Physics Communications **180**, 2582 – 2615 (2009).

[48] John P. Perdew, Kieron Burke, and Matthias Ernzerhof, "Generalized gradient approximation made simple," Phys. Rev. Lett. **77**, 3865–3868 (1996).

[49] D. R. Hamann, "Optimized norm-conserving vanderbilt pseudopotentials," Phys. Rev. B **88**, 085117 (2013).

[50] Mitsuaki Kawamura, "Fermisurfer: Fermi-surface viewer providing multiple representation schemes," Computer Physics Communications **239**, 197 – 203 (2019).

[51] J. D. Hettinger, S. E. Lofland, P. Finkel, T. Meehan, J. Palma, K. Harrell, S. Gupta, A. Ganguly, T. El-Raghy, and M. W. Barsoum, "Electrical transport, thermal transport, and elastic properties of M_2AlC (m = Ti, cr, nb, and v)," Phys. Rev. B **72**, 115120 (2005).

[52] Guobing Ying, Xiaodong He, Mingwei Li, Shanyi Du, Wenbo Han, and Fei He, "Effect of cr7c3 on the mechanical, thermal, and electrical properties of cr2alc," Journal of Alloys and Compounds **509**, 8022–8027 (2011).

[53] Wubian Tian, Peiling Wang, Guojun Zhang, Yanmei Kan, Yongxiang Li, and Dongsheng Yan, "Synthesis and thermal and electrical properties of bulk cr2alc," Scripta Materialia **54**, 841 – 846 (2006).

[54] T. Scabarozi, A. Ganguly, J. D. Hettinger, S. E. Lofland, S. Amini, P. Finkel, T. El-Raghy, and M. W. Barsoum, "Electronic and thermal properties of ti3al(c0.5,n0.5)2, ti2al(c0.5,n0.5) and ti2aln," Journal of Applied Physics **104**, 073713 (2008).

[55] Wubian Tian, Peiling Wang, Guojun Zhang, Yanmei Kan, Yongxiang Li, and Dongsheng Yan, "Synthesis and thermal and electrical properties of bulk cr2alc," Scripta Materialia **54**, 841–846 (2006).

[56] Bouchaib Manoun, R. P. Gulve, S. K. Saxena, S. Gupta, M. W. Barsoum, and C. S. Zha, "Compression behavior of m2alc (m=ti, v, cr, nb, and ta) phases to above 50 gpa," Phys. Rev.

B **73**, 024110 (2006).

[57] Zhimei Sun, Rajeev Ahuja, Sa Li, and Jochen M. Schneider, "Structure and bulk modulus of m2alc (m=ti, v, and cr)," Applied Physics Letters **83**, 899–901 (2003).

[58] Jiemin Wang, Jingyang Wang, Aijun Li, Jingjing Li, and Yanchun Zhou, "Theoretical study on the mechanism of anisotropic thermal properties of ti2alc and cr2alc," Journal of the American Ceramic Society **97**, 1202–1208 (2014).

[59] Jochen M. Schneider, Darwin P. Sigumonrong, Denis Music, Claudia Walter, Jens Emmerlich, Riza Iskandar, and Joachim Mayer, "Elastic properties of cr2alc thin films probed by nanoindentation and ab initio molecular dynamics," Scripta Materialia **57**, 1137 – 1140 (2007).

[60] S. E. Lofland, J. D. Hettinger, K. Harrell, P. Finkel, S. Gupta, M. W. Barsoum, and G. Hug, "Elastic and electronic properties of select m2ax phases," Applied Physics Letters **84**, 508–510 (2004).

[61] Sankalp Kota, Matthias Agne, Eugenio Zapata-Solvas, Olivier Dezellus, Diego Lopez, Bruno Gardiola, Miladin Radovic, and Michel W. Barsoum, "Elastic properties, thermal stability, and thermodynamic parameters of moalb," Phys. Rev. B **95**, 144108 (2017).

[62] J. S. Dugdale and Z. S. Basinski, "Mathiessen's rule and anisotropic relaxation times," Phys. Rev. **157**, 552–560 (1967).

[63] Francesco Ricci, Wei Chen, Umut Aydemir, G Jeffrey Snyder, Gian-Marco Rignanese, Anubhav Jain, and Geoffroy Hautier, "An ab initio electronic transport database for inorganic materials," Scientific Data **4**, 170085 (2017).

[64] Jamal I. Mustafa, Marco Bernardi, Jeffrey B. Neaton, and Steven G. Louie, "Ab initio electronic relaxation times and transport in noble metals," Phys. Rev. B **94**, 155105 (2016).

[65] P. Delugas, A. Filippetti, M. J. Verstraete, I. Pallecchi, D. Marré, and V. Fiorentini, "Doping-induced dimensional crossover and thermopower burst in nb-doped srtio$_3$ superlattices," Phys. Rev. B **88**, 045310 (2013).

[66] R Farris, M B Maccioni, A Filippetti, and V Fiorentini, "Influence of thermal conductivity and of non-constant relaxation time on thermoelectricity in mg3sb2," Journal of Physics: Conference Series **1226**, 012010 (2019).

[67] T. Ouisse, D. Pinek, and M.W. Barsoum, "Modelling in-plane magneto-transport in cr2alc," Ceramics International **45**, 22956 – 22960 (2019).

[68] Giorgia Fugallo and Luciano Colombo, "Calculating lattice thermal conductivity: a synopsis," Physica Scripta **93**, 043002 (2018).

[69] R. Peierls, "Zur kinetischen theorie der wrmeleitung in kristallen," Annalen der Physik **395**, 1055–1101 (1929).

[70] P. Klemens, "Thermal conductivity and lattice vibrational modes," Solid State Phys. - Adv. Res. Appl. **7**, 1–98 (1958).

[71] Joseph Callaway, "Model for lattice thermal conductivity at low temperatures," Phys. Rev. **113**, 1046–1051 (1959).

[72] J. F. Ziman, *Electrons and phonons: the theory of transport phenomena in solids* (Oxford University Press, Oxford, 2001).

[73] Andrea Cepellotti, Giorgia Fugallo, Lorenzo Paulatto, Michele Lazzeri, Francesco Mauri, and Nicola Marzari, "Phonon hydrodynamics in two-dimensional materials," Nature Communications **6**, 6400 (2015).

[74] Giorgia Fugallo, Andrea Cepellotti, Lorenzo Paulatto, Michele Lazzeri, Nicola Marzari, and Francesco Mauri, "Thermal conductivity of graphene and graphite: Collective excitations and mean free paths," Nano Letters **14**, 6109–6114 (2014).

[75] Maria Barbara Maccioni, Roberta Farris, and Vincenzo Fiorentini, "Ab initio thermal conductivity of thermoelectric mg_3sb_2: Evidence for dominant extrinsic effects," Phys. Rev. B **98**, 220301 (2018).

[76] S H Shah and P D Bristowe, "Point defect formation in M 2 AlC (M = Zr , Cr) MAX phases and their tendency to disorder and amorphize," Scientific Reports , 1–8 (2017).

[77] C. A. Ratsifaritana and P. G. Klemens, "Scattering of phonons by vacancies," International Journal of Thermophysics **8**, 737–750 (1987).